Research Article Vol. 6, No. 12 / December 2019 / Optica 1478

Emergent asymmetries and enhancement in the absorption of natural hyperbolic crystals

Xiaohu Wu,[1,2] Cameron A. McEleney,[3] Mario González-Jiménez,[4] and Rair Macêdo[5,*]

[1]Key Laboratory of 3D Micro/Nano Fabrication and Characterization of Zhejiang Province, School of Engineering, Westlake University, 18 Shilongshan Road, Hangzhou 310024, Zhejiang Province, China
[2]Institute of Advanced Technology, Westlake Institute for Advanced Study, 18 Shilongshan Road, Hangzhou 310024, Zhejiang Province, China
[3]SUPA School of Physics and Astronomy, University of Glasgow, Glasgow G12 8QQ, UK
[4]School of Chemistry, University of Glasgow, Glasgow G12 8QQ, UK
[5]James Watt School of Engineering, Electronics & Nanoscale Engineering Division, University of Glasgow, Glasgow G12 8QQ, UK
*Corresponding author: Rair.Macedo@glasgow.ac.uk

Received 25 July 2019; revised 8 October 2019; accepted 9 October 2019 (Doc. ID 373728); published 25 November 2019

The effects of the anisotropy orientation in hyperbolic media have only recently emerged as a way to control and manipulate several optical effects. Here, we show from both experimental and theoretical evidence that highly oriented-asymmetric absorption can be induced in simple crystal quartz. This can be achieved by controlling the orientation of the anisotropy with respect to the surface of the crystal at infrared regions where crystal quartz behaves as a hyperbolic medium. What is perhaps most intriguing here is that not only is the absorption asymmetric, but it can also be significantly enhanced. Finally, we also show various mechanisms through which the asymmetry in the absorption can be optimized, such as controlling the thickness of the crystal. Such phenomena are key for directional-dependent optical devices and present a pathway for engineering angle-encoded detection and sensing.

https://doi.org/10.1364/OPTICA.6.001478

1. INTRODUCTION

Absorption is an intrinsic characteristic of optical materials, and in many cases, it is engineered to be as minimal as possible, especially for transmission-based devices [1,2]. On the other hand, high—and well-defined—absorption bands can also be employed in a variety of devices including those used in sensing [3] and energy conversion [4]. More recently, with the development of metamaterials [5] and metasurfaces [6–8], the manipulation of these absorption bands has been greatly optimized. In such man-made structures, the absorption bands arise from rearranging the internal structure of the material. For instance, Ra'di and colleagues have recently found that it is possible to realize single-layered grids that exhibit total absorption when illuminated from one side but are transparent when illuminated from the other side [6]. Yazdi *et al.* proposed a bianisotropic metasurface to realize the same effect [7], and Wang *et al.* demonstrated that strong oriented-asymmetric absorption could be achieved in metasurfaces via evanescent fields [8]. These are only a few examples to illustrate the realization of asymmetric absorption via designer nanostructures with isotropic materials as their building blocks.

One interesting route to manipulating the behavior of absorption bands is to employ layered hyperbolic metamaterials. These have been theoretically suggested as a way to achieve not only asymmetric transmission [9] but also asymmetric guided waves [10–12] and perfect absorption [13–18]. This is a consequence of hyperbolic metamaterials' anisotropic nature, which is strongly related to the orientation of the materials' optical axis [19–21]. Thus, if the optical axis is neither parallel nor perpendicular to the crystal's surface, unusual wave propagation should emerge. However, little experimental work has been carried out with these metamaterials—hyperbolic or not, in fact—as their fabrication commonly requires sophisticated fabrication processes. Such complications have led to the recent conception of van der Waals structures such as hexagonal boron nitride (hBN). These are two-dimensional natural crystals that have been recently investigated as a way to control the in-plane propagation of electromagnetic waves. They have attracted significant attention over the past few years as they can support hyperbolic polaritons (HPs) [22–28]; however, most works in the field have concentrated in the configuration wherein the optical axis is perpendicular to the material surface due to the challenges of growing such atomically thin crystals. Still, their absorption and transmission are always symmetric.

More recently, but still in the field of natural hyperbolic materials, anisotropic three-dimensional crystals—which are more readily available—have enabled researchers to mimic the optical control achieved in metamaterials. This is possible by simply engineering the direction of the crystal's intrinsic anisotropy with respect to the crystal's surface. This engineering was utilized in experimental work [20] to investigate the possibility of "refraction

bending" in natural slab lenses. In that work, it was shown that rotating the anisotropy so that it is no longer perpendicular to the crystal's surface resulted in the ability to shift the focal point of these lenses.

In this work, we demonstrate experimentally and theoretically that controlling the direction of anisotropy in natural hyperbolic crystals offers a robust platform to not only engineer oriented-asymmetric absorption, but also to greatly enhance it. To demonstrate this, we performed far-infrared spectroscopy measurements as well as computer calculations using the example material crystal quartz.

2. ASYMMETRY IN HYPERBOLIC BEHAVIOR

The optical properties of dielectric hyperbolic materials of this kind are often described in terms of their permittivity tensor [29–32]. This tensor has a simple diagonal form, given by $\varepsilon(\omega) = \mathrm{diag}(\varepsilon_\perp, \varepsilon_\perp, \varepsilon_\parallel)$, when the optical axis of a hyperbolic material, such as crystal quartz, lies along the z axis and is hence perpendicular to the crystal's surface. Here $\varepsilon_\perp$ and $\varepsilon_\parallel$ represent the ordinary and extraordinary tensor components, respectively [20,30]. There are several active phonon modes in crystal quartz, from the far-infrared region all the way to the mid-infrared region. The combination of these phonon modes yields various regions wherein hyperbolic behavior can be observed (this requires $\varepsilon_\perp$ and $\varepsilon_\parallel$ to have opposite signs). This behavior is illustrated in Fig. 1(a) where we show both components of the dielectric tensor close to four infrared active phonon modes. Various regions of hyperbolic behavior are seen, either Type I or Type II as highlighted by the grey and yellow shading, respectively. Using the aforementioned permittivity tensor, we can write the well-known dispersion relation of the electromagnetic waves, with angular frequency ω, propagating in a simple uniaxial crystal as

$$\frac{k_z^{(a,b)}}{k_0} = \pm\sqrt{\varepsilon_\perp - \sin^2\theta\frac{\varepsilon_\perp}{\varepsilon_\parallel}}. \tag{1}$$

Here k_z represents the z components of the wavevector, θ is the angle of incidence, and $k_0 = \omega/c$. The superscripts a and b represent the solutions of k_z with positive and negative imaginary parts, respectively, i.e., satisfying decay at the interface for upwards and downwards wave propagation.

The formalism described above has been broadly adopted as a convention to describe the behavior of HPs [31]. However, when the optical axis is not aligned with one of the Cartesian coordinate axes, and therefore it is not parallel nor perpendicular to the crystal's surface, the permittivity tensor becomes much more complicated, gaining off-diagonal components [20]. Thus, the well-known dispersion relation given in Eq. (1) has to be modified accordingly. If we consider that the optical axis is rotated in the x–z plane by an angle φ, and hence is no longer perpendicular to the crystal's surface as shown in Fig. 1(b), then the dispersion relation given in Eq. (1) can be now rewritten as

$$\frac{k_z^{(a,b)}}{k_0} = \frac{\sin\theta(\varepsilon_\parallel - \varepsilon_\perp)\sin\varphi\cos\varphi \pm \sqrt{\xi}}{\varepsilon_\parallel\cos^2\varphi + \varepsilon_\perp\sin^2\varphi}, \tag{2}$$

with

$$\xi = \varepsilon_\parallel\varepsilon_\perp(\varepsilon_\parallel\cos^2\varphi + \varepsilon_\perp\sin^2\varphi - \sin^2\theta).$$

Here the angle φ represents the angle by which the optical axis is rotated with respect to the z axis. This angle has been recently referred to as the "bending angle." This is because, if the optical axis is not parallel nor perpendicular to the surface of the crystal slab, it can be used to shift or "bend" the refracted beam further than it normally would—this is also a way to laterally shift or "bend" the focal point of slab lenses [20]. We should note that because the effect of this bending angle φ is contained in the permittivity tensor, the definitions of the incident angle, incidence plane, and coordinate system shown in Fig. 1(b) do not need to be modified if φ is nonzero.

Here, the wavevector component along the z axis has both positive and negative imaginary parts, which are associated with the propagation of upwards and downwards waves, respectively, following the notations of the incidence geometry shown in

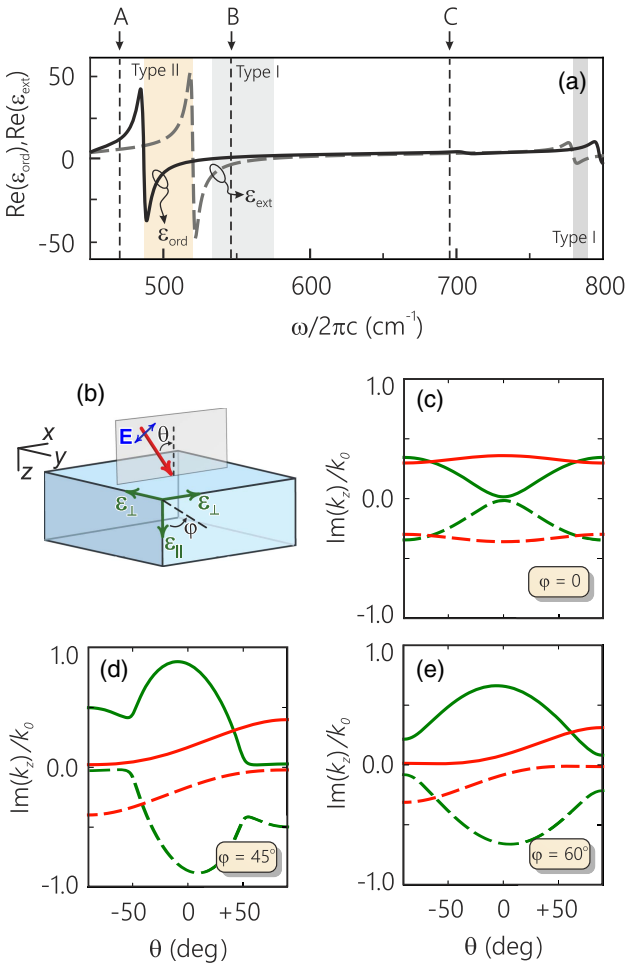

Fig. 1. (a) Real part of the components of the dielectric tensor of crystal quartz along its ordinary ($\varepsilon_\perp$) and extraordinary ($\varepsilon_\parallel$) axes showing the regions where the crystal behaves as either hyperbolic Type I (grey shading) or Type II (yellow shading). (b) Schematics of the incidence of radiation onto a crystal quartz surface. The plane of incidence is in the x–z plane with incidence angle denoted as θ. The anisotropy, represented by $\varepsilon_\parallel$, is originally along z, but it is allowed to rotate in the x–z plane. This rotation is controlled by the "bending angle" φ. The imaginary part of k_z is given for (c) $\varphi = 0$, (d) $\varphi = 45°$, and (e) $\varphi = 60°$. The green lines are for $\omega = 545$ cm^{-1}, and the red lines are for $\omega = 695$ cm^{-1}. The solid lines are for $k_z^{(a)}$, and the dashed lines are for $k_z^{(b)}$. Note that these are equivalent to the isofrequency curves usually given for hyperbolic materials (k_x versus k_z). However, in order to compare with the data that will follow, we have used the relation $k_x = k_0 \sin\theta$ in the x axis.

Fig. 1(b). In general, high and low values of $\mathrm{Im}(k_z)$ indicate high and low absorption, respectively. Thus, in Figs. 1(c)–1(e) we look at the behavior of this quantity for various cases as a way to understand how to induce changes, and even control the absorption, through simple changes in the anisotropy direction. These curves are plotted from Eq. (2) at two infrared frequencies: the green lines are for $\omega = 545\ \mathrm{cm}^{-1}$, and the red lines are for $\omega = 695\ \mathrm{cm}^{-1}$. From these, we can see that when the optical axis lies along z, $\mathrm{Im}(k_z)$ is symmetric in θ, and hence k_x [see Fig. 1(c)]. However, such behavior does not persist when the optical axis is at an arbitrary angle with the surface ($0 < \varphi < 90°$) as shown in Fig. 1(d) for $\varphi = 45°$. The asymmetry seen in this case dramatically changes with the bending angle as shown in Fig. 1(e) when $\varphi = 60°$. Thus, we expect that this asymmetry in $\mathrm{Im}(k_z)$ will lead to asymmetric absorption for positive and negative incident angles. It is noteworthy that the amplitude of $\mathrm{Im}(k_z)$ increases when comparing Fig. 1(c) with 1(e). Similar behavior has been pointed out by Nefedov *et al.* in artificial multilayered structures, and it was then described as a mechanism through which it is possible to realize perfect absorption [14,15].

3. RESULTS

A. Infrared Spectroscopy Measurements

In order to investigate the effect of the anisotropy orientation on the absorption bands of crystal quartz, we performed Fourier transform infrared spectroscopy measurements of the transmissivity tt^* and reflectivity rr^* using a Bruker Vertex 70 spectrometer. Our spectra have a resolution of 2 cm^{-1}, and each spectrum was averaged 16 times. We used a KRS-5 polarizer placed in the beam path to obtain p-polarized radiation for all measurements. The absorption was then calculated using the relation $1 - rr^* - tt^*$ for both theoretical and experimental spectra. The samples used were flat slabs of chemically polished crystal quartz with a thickness of $d = 25\ \mu\mathrm{m}$ and a diameter of 20 mm. These were obtained from Boston Piezo Optics Inc. The orientation of the anisotropy axis was chosen with respect to the crystal's surface, being precisely determined by single-crystal x-ray diffraction measurements with the crystal mounted on a goniometer, which allowed for the positioning of the crystal at selected orientations.

B. Asymmetric Absorption

The absorption of crystal quartz as a function of both the incident angle θ and bending angle φ is shown in Fig. 2. When $\varphi = 0$, the absorption is symmetric on θ as shown in Figs. 2(a)–2(c). In part (a) we show the calculated absorption maps as a function of both frequency and incident angle, and in parts (b)–(c) we show the comparison between theoretical and experimental spectra at two different incident angles, $\pm 30°$ and $\pm 60°$. This behavior dramatically changes when φ is at an arbitrary angle with respect to the crystal surface. It is then possible to induce extreme asymmetries on the absorption as shown in Figs. 2(d)–2(f) for $\varphi = 45°$. In part (f) we show experimental and theoretical lines, which illustrate particularly high large asymmetry at high incidences angles of $\theta = \pm 60°$. For instance, at $\omega = 545\ \mathrm{cm}^{-1}$ (marked as B) the absorption goes from being very small at $\theta = +60°$ to near perfect at $\theta = -60°$. Similar behavior can be observed at much higher frequencies [$\omega = 695\ \mathrm{cm}^{-1}$ marked as C in Figs. 2(g)–2(i)] if the bending angle is now $\varphi = \pm 60°$. In all these cases, the angular-asymmetric absorption stems from the asymmetric propagation waves and

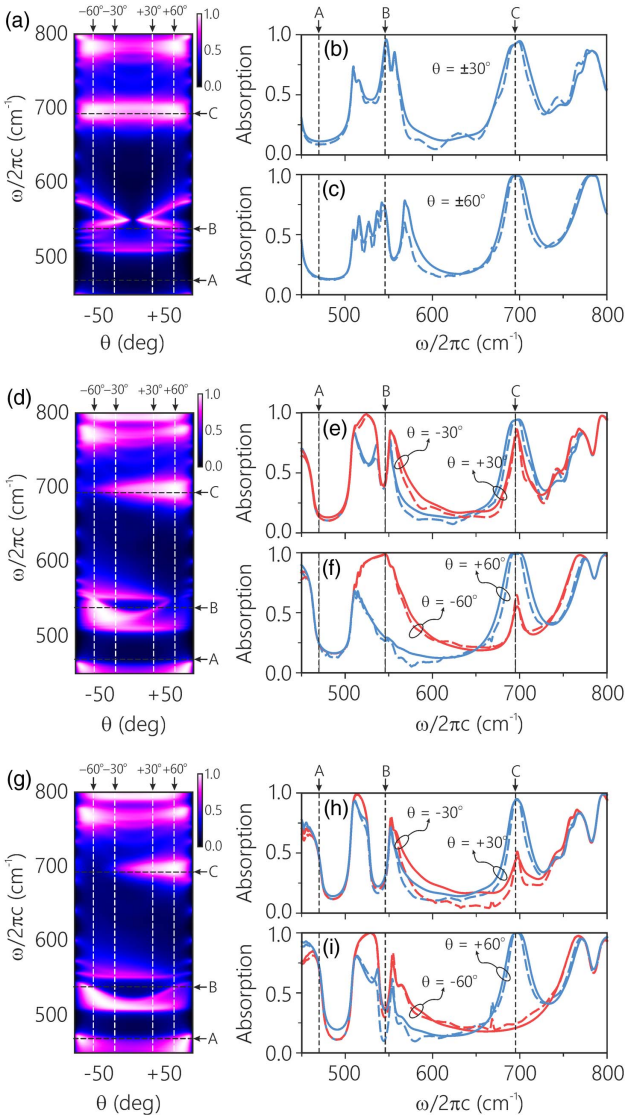

Fig. 2. Absorption in crystal quartz for various orientations of the anisotropy with respect to the crystal's surface given by (a)–(c) $\varphi = 0$, (d)–(f) $\varphi = 45°$, and (g)–(i) $\varphi = 60°$. The panels to the left show theoretical absorption maps as a function of both the incident angle θ and frequency of the incident radiation ω. The panels to the right show a comparison between experimental (dashed lines) and theoretical (solid lines) spectra for $\theta = \pm 30°$ and $\theta = \pm 60°$, highlighting the orientation-dependent asymmetry. Since the angles of incidence for the measured spectra are manually adjusted within the spectrometer, the experimental lines (dashed) have an estimated $\pm 2°$ error.

the behavior of $\mathrm{Im}(k_z)$. In particular, the behavior shown here for frequencies A, B, and C can be directly associated with the asymmetries in the values of $\mathrm{Im}(k_z)$ shown in Figs. 1(c)–1(e) supported by the change in the direction of the anisotropy.

The asymmetries in absorption can be better understood by taking a closer took at their behavior at individual frequencies. In Figs. 3(a) and 3(b), for example, we show the absorption of crystal quartz at $\omega = 545\ \mathrm{cm}^{-1}$ (frequency B) as a function of θ and φ. The calculated absorption line for $\varphi = 45°$ shows that while perfect absorption is achieved at high negative incident angles, minimal absorption is seen at their positive counterparts. To further probe this, we show in Fig. 3(c) the isofrequency curves

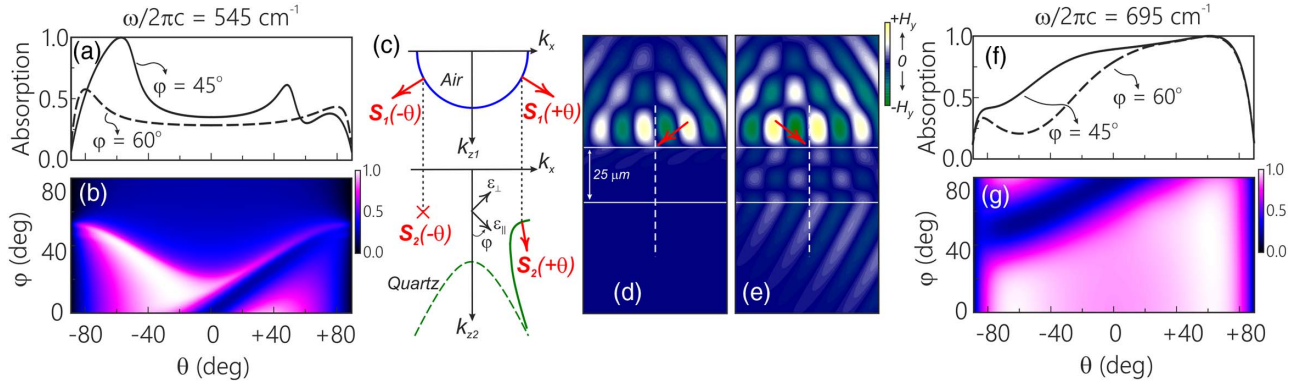

Fig. 3. (a) Absorption lines as a function of the incident angle θ calculated at the frequency highlighted in Fig. 2 as B ($\omega = 545$ cm^{-1}) for two bending angles previously discussed ($\varphi = 45°$ and $\varphi = 60°$). (b) Map showing the behavior of the absorption as a function of both incident angle θ and bending angle φ also at frequency B. Isofrequency curves [dispersion curves of Re(k_z)] are shown in (c) for air and quartz at $\varphi = 45°$ and at frequency B—note that the dashed green line shows the standard hyperbolic dispersion of crystal quartz at $\varphi = 0$ for comparison with the dispersion at $\varphi = 45°$ (solid green line). The directions of the Poynting vectors inside and outside the crystal are also shown as red arrows for $\theta = \pm 60°$. Respective instantaneous H_y field of a *p*-polarized Gaussian beam passing through a quartz crystal of thickness 25 μm incident at (d) $\theta = -60°$ and (e) $\theta = +60°$. (f) Absorption lines and (g) absorption map at frequency C are shown for comparison to those given in parts (a) and (b), respectively.

(also referred to as equifrequency plots, or dispersion relations) for air and crystal quartz with $\varphi = 45°$ (and $\varphi = 0$ as a dashed line for reference of the simple case). We can see that while a solution of Re(k_z) is found for positive incident angles ($+k_x$), no solution is seen for negative incident angles ($-k_x$). No solution for Re(k_z) means that no propagation is allowed in the material. This behavior is shown in Figs. 3(d) and 3(e) with the instantaneous value of H_y, which shows the behavior of the wave fronts as a Gaussian beam passes through a crystal quartz slab of 25 μm thickness (details of the calculations of the fields of a refracted beam are given in Refs. [33,34]). For $\theta = -60°$, nothing gets through the material as shown in Fig. 3(d), while for $\theta = +60°$ radiation is allowed to travel through as seen in Fig. 3(e)—both in agreement with Fig. 3(a)—and the direction of the refracted beam in Fig. 3(e) is also in agreement with that shown in Fig. 3(c) as S_2 ($+\theta$). From Fig. 3(a), we can also see that as the bending angle is increased to $\varphi = 60°$, the asymmetry in the absorption seen for $\varphi = 45°$ can be completely destroyed. In Figs. 3(f) and 3(g), we show similar data to that in Figs. 3(a)–3(b) but now at a higher frequency $\omega = 695$ cm^{-1} (frequency C). This shows that the reverse behavior is now achieved, where high absorption is seen at $+\theta$ and low absorption is seen at $-\theta$. As discussed previously, the absorption has a strong relationship with Im(k_z). Thus, this behavior is related to those discussed in Fig. 1(d) and 1(e).

C. Enhanced and Optimal Absorption

Up to this point, we have only discussed how to use the anisotropy orientation in order to induce highly asymmetric absorption in the natural hyperbolic crystal quartz. However, as pointed out by Nefedov *et al.* [14,15] and Wu *et al.* [2,17,18], this can also be a way to greatly enhance the absorption bands in tilted anisotropic metamaterials. Since the growth of such structures is experimentally challenging, we will now look at how this can be applied to natural materials.

In Fig. 4(a) we give the absorption of crystal quartz as a function of the incident angle for three bending angles at $\omega = 470$ cm^{-1} (marked as A in Fig. 2). One can see that absorption is greatly enhanced as the bending angle is increased from 0 to 45°. Further

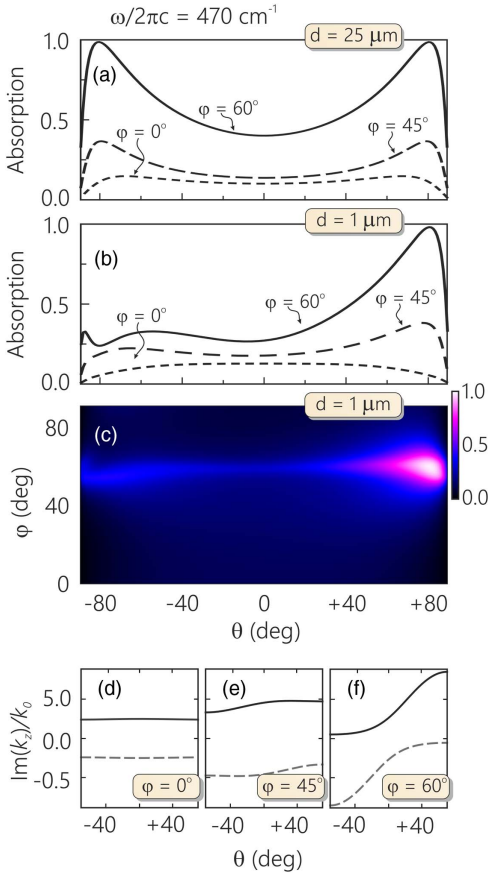

Fig. 4. Enhancement of the absorption calculated at $\omega = 470$ cm^{-1} [frequency marked as A in Fig. 1(a)] in a crystal quartz sample. In (a) the enhancement is given by increasing the bending angle φ for a sample of thicknesses $d = 25$ μm. In (b) the asymmetry enhancement is given by decreasing the thickness of the crystal, which is now taken to be $d = 1$ μm. (c) More details of the asymmetry as a function of both incidence angle θ and bending angle φ. The imaginary part of the wavevector component k_z at this frequency is also given for (d) $\varphi = 0$, (e) $\varphi = 45°$, and (f) $\varphi = 60°$.

increasing the bending angle to 60° results in, at high incident angles, near-perfect absorption. The absorption is smaller than 0.15 for all the incident angles when the anisotropy axis is along the z axis, while perfect absorption can be realized at incident angles around ±80° when the bending angle is 60°. This enhancement can be finely controlled through the sample thickness as shown in Fig. 4(b). Decreasing the sample thickness from 25 μm, as shown in Fig. 4(a), to 1 μm, as shown in Fig. 4(b), can be used as a way to optimize the bands to a point where near-perfect absorption can be found. However, the absorption is now highly asymmetric, as most radiation is being absorbed at high positive incident angles, but relatively low absorption is seen for their negative counterparts. A more comprehensive picture of this can be seen in Fig. 4(c), where we show the evolution of the absorption as a function of both incident angle θ and bending angle φ.

The enhanced absorption shown in Fig. 4(a)–4(c) is also attributed to an enhancement of the imaginary part of the wavevector [13–15]. In Figs. 4(d)–4(f) we show the values of $\mathrm{Im}(k_z)$ for the bending angles of interest, and it is seen that as φ increases so does $\mathrm{Im}(k_z)$ as expected from Fig. 4(a). However, at high values of ϕ, large asymmetry is seen, which is not obvious in thick samples but evident in thinner ones. This is because, for a thinner sample, the effect of backwards waves (internally reflected) is not as prominent, so the absorption reflects the asymmetry seen in k_z, while in a thick sample, both waves have to be considered, and thus only an enhancement of absorption is seen in Fig. 4(a).

4. DISCUSSION AND CONCLUSIONS

In summary, we have used the example of crystal quartz to demonstrate that strong angular-asymmetric absorption can be achieved in simple uniaxial crystals due to asymmetric wave propagation. This can be achieved by controlling the direction of the anisotropy and, in doing so, the absorption can reach maximal value for waves incident in one particular direction while being minimal for waves incident in the opposite direction. Compared with other nanostructures, in particular those that have been designed to exhibit angular-asymmetric absorption [8], our material is much simpler and has no complicated fabrication techniques. Here we also demonstrated that through the same method absorption can be enhanced. We believe that such simple crystalline materials may find important applications in unidirectional emission [35] and energy conversion [4]. We should mention that while the control of HPs has recently been extensively investigated in natural van der Waals structures, their response is always symmetric. Also, due to limited fabrication capabilities at present, the impact of the optical axis in such media has not yet been addressed.

Finally, the method discussed here can be readily applied to achieve similar behavior in previously studied hyperbolic materials by controlling their anisotropy direction with respect to the material's surface. While the control of the absorption here was done through cutting crystals with different anisotropy orientations with respect to their surfaces, tunability of the bending angle should be possible through using external fields in other hyperbolic materials such as nematic liquid crystals [36].

Funding. Leverhulme Trust (RPG-2018-350); Carnegie Trust for the Universities of Scotland; Engineering and Physical Sciences Research Council (EP/N007417/1).

Acknowledgment. This work was financially supported by the Leverhulme Trust and the University of Glasgow through LKAS funds. The work of C. A. McEleney was supported by the Carnegie Trust for the Universities of Scotland. M. González-Jiménez gratefully acknowledges support through EPSRC grant EP/N007417/1 and Leverhulme grant RPG-2018-350.

REFERENCES

1. Y. Zhang, Q. Du, C. Wang, T. Fakhrul, S. Liu, L. Deng, D. Huang, P. Pintus, J. Bowers, C. A. Ross, J. Hu, and L. Bi, "Monolithic integration of broadband optical isolators for polarization-diverse silicon photonics," Optica **6**, 473–478 (2019).
2. X. Wu, "High extinction ratio hexagonal boron nitride polarizer," Optik **175**, 290–295 (2018).
3. C. Ranacher, C. Consani, A. Tortschanoff, R. Jannesari, M. Bergmeister, T. Grille, and B. Jakoby, "Mid-infrared absorption gas sensing using a silicon strip waveguide," Sens. Actuators A **277**, 117–123 (2018).
4. Y. Xie, X. Fan, J. D. Wilson, R. N. Simons, Y. Chen, and J. Q. Xiao, "A universal electromagnetic energy conversion adapter based on a metamaterial absorber," Sci. Rep. **4**, 6301 (2014).
5. G. Duan, J. Schalch, X. Zhao, J. Zhang, R. D. Averitt, and X. Zhang, "Identifying the perfect absorption of metamaterial absorbers," Phys. Rev. B **97**, 035128 (2018).
6. Y. Ra'di, V. S. Asadchy, and S. A. Tretyakov, "Total absorption of electromagnetic waves in ultimately thin layers," IEEE Trans. Antennas Propag. **61**, 4606–4614 (2013).
7. M. Yazdi, M. Albooyeh, R. Alaee, V. Asadchy, N. Komjani, C. Rockstuhl, C. R. Simovski, and S. Tretyakov, "A bianisotropic metasurface with resonant asymmetric absorption," IEEE Trans. Antennas Propag. **63**, 3004–3015 (2015).
8. X. Wang, A. Díaz-Rubio, V. S. Asadchy, G. Ptitcyn, A. A. Generalov, J. Ala-Laurinaho, and S. A. Tretyakov, "Extreme asymmetry in metasurfaces via evanescent fields engineering: angular-asymmetric absorption," Phys. Rev. Lett. **121**, 256802 (2018).
9. G. B. Smith, "Theory of angular selective transmittance in oblique columnar thin films containing metal and voids," Appl. Opt. **29**, 3685–3693 (1990).
10. D. P. G. Russo and J. H. Harris, "Wave propagation in anisotropic thin-film optical waveguides," J. Opt. Soc. Am. **63**, 138–145 (1973).
11. A. Knoesen, M. Moharam, and T. Gaylord, "Electromagnetic propagation at interfaces and in waveguides in uniaxial crystals," Appl. Phys. B **38**, 171–178 (1985).
12. A. D. Boardman, P. Egan, and M. McCall, "Optic axis-driven new horizons for hyperbolic metamaterials," EPJ Appl. Metamater. **2**, 11 (2015).
13. S. M. Hashemi and I. S. Nefedov, "Wideband perfect absorption in arrays of tilted carbon nanotubes," Phys. Rev. B **86**, 195411 (2012).
14. I. S. Nefedov, C. A. Valagiannopoulos, S. M. Hashemi, and E. I. Nefedov, "Total absorption in asymmetric hyperbolic media," Sci. Rep. **3**, 2662 (2013).
15. I. S. Nefedov, C. A. Valagiannopoulos, and L. A. Melnikov, "Perfect absorption in graphene multilayers," J. Opt. **15**, 114003 (2013).
16. X. Wu and C. Fu, "Ultra-broadband perfect absorption with stacked asymmetric hyperbolic metamaterial slabs," Nanoscale Microscale Thermophys. Eng. **22**, 114–123 (2018).
17. X. Wu and C. Fu, "Manipulation of enhanced absorption with tilted hexagonal boron nitride slabs," J. Quant. Spectrosc. Radiat. Transfer **209**, 150–155 (2018).
18. X. Wu, "Perfect absorption in cascaded asymmetric hyperbolic metamaterial slabs," Superlattices Microstruct. **124**, 10–16 (2018).
19. X. Wu, C. Fu, and Z. M. Zhang, "Effect of orientation on the directional and hemispherical emissivity of hyperbolic metamaterials," Int. J. Heat Mass Transfer **135**, 1207–1217 (2019).
20. R. Macêdo, T. Dumelow, R. E. Camley, and R. L. Stamps, "Oriented asymmetric wave propagation and refraction bending in hyperbolic media," ACS Photon. **5**, 5086–5094 (2018).
21. R. Macêdo and R. E. Camley, "Engineering terahertz surface magnon-polaritons in hyperbolic antiferromagnets," Phys. Rev. B **99**, 014437 (2019).

22. S. Dai, Z. Fei, Q. Ma, A. S. Rodin, M. Wagner, A. S. McLeod, M. K. Liu, W. Gannett, W. Regan, K. Watanabe, T. Taniguchi, M. Thiemens, G. Dominguez, A. H. C. Neto, A. Zettl, F. Keilmann, P. J. Herrero, M. M. Fogler, and D. N. Basov, "Tunable phonon polaritons in atomically thin van der Waals crystals of boron nitride," Science **343**, 1125–1129 (2014).
23. J. D. Caldwell, A. V. Kretinin, Y. Chen, V. Giannini, M. M. Fogler, Y. Francescato, C. T. Ellis, J. G. Tischler, C. R. Woods, A. J. Giles, M. Hong, K. Watanabe, T. Taniguchi, S. A. Maier, and K. S. Novoselov, "Sub-diffractional volume-confined polaritons in the natural hyperbolic material hexagonal boron nitride," Nat. Commun. **5**, 5221 (2014).
24. T. Low, A. Chaves, J. D. Caldwell, A. Kumar, N. X. Fang, P. Avouris, T. F. Heinz, F. Guinea, L. M. Moreno, and F. Koppens, "Polaritons in layered two-dimensional materials," Nat. Mater. **16**, 182 (2017).
25. K. Korzeb, M. Gajc, and A. Pawlak, "Compendium of natural hyperbolic materials," Opt. Express **23**, 25406–25424 (2015).
26. J. Sun, N. M. Litchinitser, and J. Zhou, "Indefinite by nature: from ultraviolet to terahertz," ACS Photon. **1**, 293–303 (2014).
27. D. G. Baranov, J. H. Edgar, T. Hoffman, N. Bassim, and J. D. Caldwell, "Perfect interferenceless absorption at infrared frequencies by a can der Waals crystal," Phys. Rev. B **92**, 20145 (2015).
28. T. G. Folland, T. W. W. Maß, J. R. Matson, J. R. Nolen, S. Liu, K. Watanabe, T. Taniguchi, J. H. Edgar, T. Taubner, and J. D. Caldwell, "Probing hyperbolic polaritons using infrared attenuated total reflectance micro-spectroscopy," MRS Commun. **8**, 1418–1425 (2018).
29. R. Rodrigues da Silva, R. Macêdo, T. Dumelow, J. A. P. da Costa, S. B. Honorato, and A. P. Ayala, "Using phonon resonances as a route to all-angle negative refraction in the far-infrared region: the case of crystal quartz," Phys. Rev. Lett. **105**, 163903 (2010).
30. R. Estevâm da Silva, R. Macêdo, T. Dumelow, J. A. P. da Costa, S. B. Honorato, and A. P. Ayala, "Far-infrared slab lensing and subwavelength imaging in crystal quartz," Phys. Rev. B **86**, 155152 (2012).
31. A. Poddubny, I. Iorsh, P. Belov, and Y. Kivshar, "Hyperbolic metamaterials," Nat. Photonics **7**, 948 (2013).
32. S. Foteinopoulou, G. C. R. Devarapu, G. S. Subramania, S. Krishna, and D. Wasserman, "Phonon-polaritonics: enabling powerful capabilities for infrared photonics," Nanophotonics (to be published).
33. R. Macêdo, R. R. da Silva, T. Dumelow, and J. A. P. da Costa, "MgF_2 as a material exhibiting all-angle negative refraction and subwavelength imaging due to the phonon response in the far infrared," Opt. Commun. **310**, 94–99 (2014).
34. R. Macêdo and T. Dumelow, "Beam shifts on reflection of electromagnetic radiation off anisotropic crystals at optic phonon frequencies," J. Opt. **15**, 014013 (2013).
35. S. Inampudi, J. Cheng, M. M. Salary, and H. Mosallaei, "Unidirectional thermal radiation from a sic metasurface," J. Opt. Soc. Am. B **35**, 39–46 (2018).
36. G. Pawlik, K. Tarnowski, W. Walasik, A. C. Mitus, and I. C. Khoo, "Liquid crystal hyperbolic metamaterial for wide-angle negative and positive refraction and reflection," Opt. Lett. **39**, 1744–1747 (2014).